

THE *GALEX*/S⁴G UV–IR COLOR–COLOR DIAGRAM: CATCHING SPIRAL GALAXIES AWAY FROM THE BLUE SEQUENCE

ALEXANDRE Y. K. BOUQUIN¹, ARMANDO GIL DE PAZ¹, SAMUEL BOISSIER^{2,3}, JUAN-CARLOS MUÑOZ-MATEOS⁴, KARTIK SHETH⁵, DENNIS ZARITSKY⁶, JARKKO LAINE⁷, JESÚS GALLEGÓ¹, REYNIER F. PELETIER⁸, BENJAMIN R. RÖCK^{9,10}, AND JOHAN H. KNAPEN^{9,10}

¹Departamento de Astrofísica y CC. de la Atmósfera, Universidad Complutense de Madrid, E-28040 Madrid, Spain; abouquin@fis.ucm.es

²Aix Marseille Université, CNRS, LAM (Laboratoire d’Astrophysique de Marseille) UMR 7326, F-13388 Marseille, France

³I.N.A.F., Osservatorio Astronomico di Bologna, via Ranzani 1 I-40127 Bologna, Italy

⁴European Southern Observatory, Casilla 19001, Santiago 19, Chile

⁵National Radio Astronomy Observatory/NAASC, 520 Edgemont Road, Charlottesville, VA 22903, USA

⁶Steward Observatory, University of Arizona, 933 North Cherry Avenue, Tucson, AZ 85721, USA

⁷Astronomy Division, Department of Physics, University of Oulu, P.O. Box 3000, FIN-90014 Oulu, Finland

⁸Kapteyn Astronomical Institute, Postbus 800, NL-9700 AV Groningen, The Netherlands

⁹Instituto de Astrofísica de Canarias, Vía Láctea, S/N, E-38205 La Laguna, Spain

¹⁰Departamento de Astrofísica, Universidad de La Laguna, E-38205 La Laguna, Tenerife, Spain

Received 2014 December 22; accepted 2015 January 24; published 2015 February 12

ABSTRACT

We obtained *GALEX* FUV, NUV, and *Spitzer*/IRAC 3.6 μm photometry for >2000 galaxies, available for 90% of the S⁴G sample. We find a very tight *GALEX* blue sequence (GBS) in the (FUV–NUV) versus (NUV–[3.6]) color–color diagram, which is populated by irregular and spiral galaxies, and is mainly driven by changes in the formation timescale (τ) and a degeneracy between τ and dust reddening. The tightness of the GBS provides an unprecedented way of identifying star-forming galaxies and objects that are just evolving to (or from) what we call the *GALEX* green valley (GGV). At the red end of the GBS, at (NUV–[3.6]) > 5, we find a wider *GALEX* red sequence (GRS) mostly populated by E/S0 galaxies that has a perpendicular slope to that of the GBS and of the optical red sequence. We find no such dichotomy in terms of stellar mass (measured by $M_{[3.6]}$) since both massive ($M_* > 10^{11} M_\odot$) blue- and red-sequence galaxies are identified. The type that is proportionally more often found in the GGV is the S0–Sa’s, and most of these are located in high-density environments. We discuss evolutionary models of galaxies that show a rapid transition from the blue to the red sequence on a timescale of 10^8 yr.

Key words: galaxies: evolution – galaxies: photometry – galaxies: star formation

1. INTRODUCTION

Color–magnitude and color–color diagrams are proven galaxy evolution diagnostic tools. Recent studies making use of *GALEX* and SDSS data, such as Wyder et al. (2007), have clearly shown the existence of a bimodal distribution of galaxies in (NUV– r) versus r color–magnitude diagrams (CMDs), where the redder and brighter region is populated mainly by early-type galaxies in a “red sequence,” and where the bluer and fainter part of the diagram is populated mainly by late-type galaxies in a “blue sequence.”

We construct a color–magnitude and a color–color diagram using far-UV (FUV; effective wavelength 151.6 nm) and near-UV (NUV; 226.7 nm) images from *GALEX* (Martin et al. 2005) and 3.6 μm images from the images released by the *Spitzer* Survey of Stellar Structure in Galaxies (S⁴G; Sheth et al. 2010). The near-IR (NIR) band is sensitive mainly to old stars and the UV bands to young stars (<1 Gyr). As we show below, a combination of UV and NIR bands allows us to separate star-forming from passively evolving galaxies, while the use of the two *GALEX* UV bands makes this analysis very sensitive to transitional galaxies and to the transition timescale, as the FUV band is most sensitive to the presence of young (OB-type) stars. Our sample is based on the *Spitzer* Survey of Stellar Structure in Galaxies (S⁴G; Sheth et al. 2010). In this study, we gather the publicly available *GALEX* data (from data release GR6/7) for these S⁴G galaxies and measure NUV and FUV surface and asymptotic photometry for over 2000 galaxies (~90% of the S⁴G galaxies). We then combine this with consistent surface and asymptotic 3.6 μm photometry from

S⁴G. We adopt a value of $H_0 = 75 \text{ km s}^{-1} \text{ Mpc}^{-1}$ for galaxies lacking a redshift-independent distance measurement (as in Sheth et al. 2010).

2. SAMPLE

The S⁴G is a volume-limited ($d < 40 \text{ Mpc}$), magnitude-limited ($m_{\text{Bcorr}} < 15.5 \text{ mag}$, corrected for inclination, galactic extinction, and K correction), and size-limited ($D_{25} > 1'$) survey avoiding the galactic equatorial plane ($|b| > 30^\circ$) of 2352 galaxies, consisting of 3.6 and 4.5 μm IRAC-band images. Galaxies covered by this survey account for the majority of the significantly sized galaxies in our extragalactic neighborhood, including galaxies of all Hubble types and masses, in various environments from field to clusters of galaxies (including 187 Virgo galaxies). The HI 21 cm redshift selection, however, biases the sample against very massive early-type galaxies (ETGs¹¹; Lagos et al. 2014). We compiled a subsample of corresponding *GALEX* (data release GR6/7) tiles using *GALEXView*¹², in both FUV and NUV for over 2100 galaxies.

FUV and NUV asymptotic magnitudes were obtained using the same method as in Gil de Paz et al. (2007), corrected for the Milky Way foreground attenuation and measured for 2053 galaxies. After excluding shallow observations with magnitude errors larger than unity and bad photometry due to

¹¹ An extension of the S⁴G sample, aimed to correct for the HI selection effect, is currently in progress.

¹² <http://galex.stsci.edu/GalexView/>

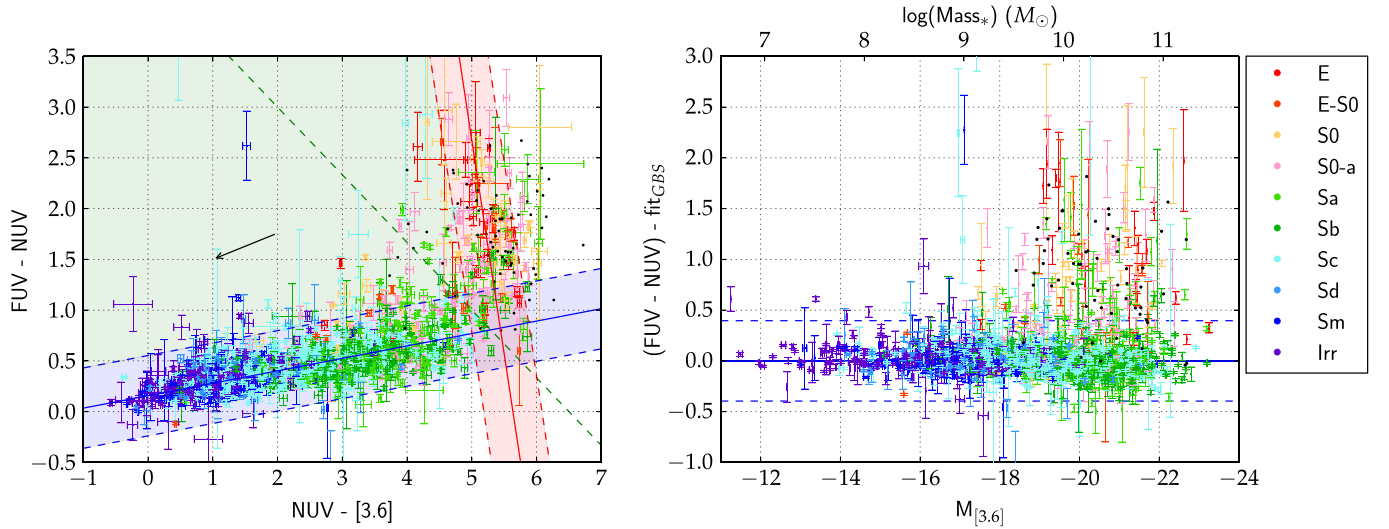


Figure 1. Left : (FUV-NUV) vs. (NUV-[3.6]) color-color diagram. Morphological types are represented by color (see the legend). We define the blue and red sequence by dividing the plot into two regions and fitting a least squares 1D polynomial (a line) to each region. The solid blue line is the weighted-by-error linear fit for the lower left region, and the solid red line is the weighted-by-error linear fit for the upper right region. The dashed lines are parallel to their solid counterpart, but translated in the (FUV-NUV) direction by $\pm 2\sigma$ for the GBS (blue shaded region), and translated in the (NUV-[3.6]) direction by $\pm 1\sigma$ for the GRS (red shaded region). The GGV is also shown (green shaded region). The black arrow indicates the reddening vector for an attenuation of $A_V = 0.5$ mag. The black dots are measurements for the Cappellari et al. (2013) sample (Section 3.2; not included in the statistics) obtained by Zaritsky et al. (2015; we adopted here $(I-[3.6]) = 0.5$ mag). We use a $3.6 \mu\text{m}$ stellar mass-to-light ratio $Y_{3.6} = 0.6$ or $\log(Y_{3.6}) = -0.22$ (IMF: Chabrier; Meidt et al. 2014). Right: color-magnitude diagram using the difference between (FUV-NUV) color and the fit to the GBS in the color-color diagram vs. $M_{[3.6]}$. Same color-coding as in the left panel.

contamination from bright stars, we are left with 1931 galaxies. The S⁴G $3.6 \mu\text{m}$ photometry has been obtained using an identical procedure but adapted to the specifics of IRAC (J. C. Muñoz-Mateos et al. 2015, in preparation). All magnitudes throughout this paper are given in the AB system. Numerical morphological types, absolute B -band magnitudes, and optical colors were obtained from HyperLeda (Paturel et al. 2003). The total UV coverage of our parent S⁴G sample is $\sim 90\%$, with a rather uniform fraction across all properties including absolute B -band magnitude, distance, and morphological types, and therefore represents and inherits the selection criteria of S⁴G.

3. RESULTS AND ANALYSIS

3.1. UV-IR Color-Color Diagram

Using the asymptotic photometry described above, we construct the (FUV-NUV) versus (NUV-[3.6]) color-color diagram (Figure 1). We find a clear bimodal pattern: a very tight blue sequence, which we call the *GALEX* blue sequence (GBS), and a less tight red sequence we call the *GALEX* red sequence (GRS). The distribution of the GRS is perpendicular to that seen in optical color-color diagrams (e.g., Strateva et al. 2001), likely due to the mass and metallicity dependence of the UV upturn (Boselli et al. 2005). The more massive and metal rich a galaxy is, the more important the contribution from the UV upturn to the UV emission and bluer the (FUV-NUV) color. Alternative uses of this color are still being explored (e.g., Hernández-Pérez and Bruzual 2014; Zaritsky et al. 2014, 2015).

To quantify the GBS and the GRS, we split the color-color plane by choosing a line that passes through coordinates (2,3) and (5,1) (left panel of Figure 1). We fit the bluer half with a simple error-weighted linear regression (the subsample size here is 1787 galaxies), giving us a slope of 0.12 ± 0.01 and a y intercept at 0.16 ± 0.01 . The standard deviation of the sample

over this range is $\text{rms}_{\text{GBS}} = 0.20$, while a Gaussian fit to the residuals yields an even smaller value of $\sigma_{\text{GBS}} = 0.10$.

We also fit the redder half (144 galaxies) with a simple error-weighted linear regression (in the (NUV-[3.6]) direction), giving us a slope of -4.21 ± 1.62 and an $\text{rms}_{\text{GRS}} = 0.45$. The location of galaxies in this diagram is strongly correlated with the Hubble type (see also Figure 4). There are only two true ellipticals in the GBS, ESO 548-023 and NGC 855. Some of the ellipticals found in the GBS are actually BCDs morphologically misclassified as ellipticals. The latter plus the 31 later-typed ETGs (E-S0,S0) located in the GBS either could be in the tail of star formation (Bresolin 2013) or could be rejuvenated systems (Kannappan et al. 2009; Thilker et al. 2010). Finally, early-type spiral galaxies (S0-a, Sa, Sab) are populating the GBS, the GRS, and the region in between (which we name *GALEX* green valley, GGV), which is consistent with a scenario where these galaxies are transitional objects.

3.2. UV-IR Color-Magnitude Diagram

Figure 1 (right) shows the residuals of the UV color to the GBS linear fit obtained in our UV-IR color-color diagram (left), $(\text{FUV-NUV}) - (\text{FUV-NUV})_{\text{GBS}}$, as a fraction of the absolute magnitude at $3.6 \mu\text{m}$, $M_{[3.6]}$, and stellar mass measured assuming a $Y_{3.6}$ of $0.6 M_{\odot}/L_{\odot}$ (Meidt et al. 2014; B. R. Röck et al. 2015, in preparation). Stellar mass is not the driver for the evolution of these systems in or out the GBS. The distribution of our samples of ETGs (our data and those from Zaritsky et al. 2015) is similar, meaning that the bias against HI-poor ETGs in S⁴G is not driving our results.

3.3. Optical Color-Magnitude Diagram

In Figure 2, we show the optical CMD, commonly used to study galaxy evolution (e.g., Faber et al. 2007). We show the

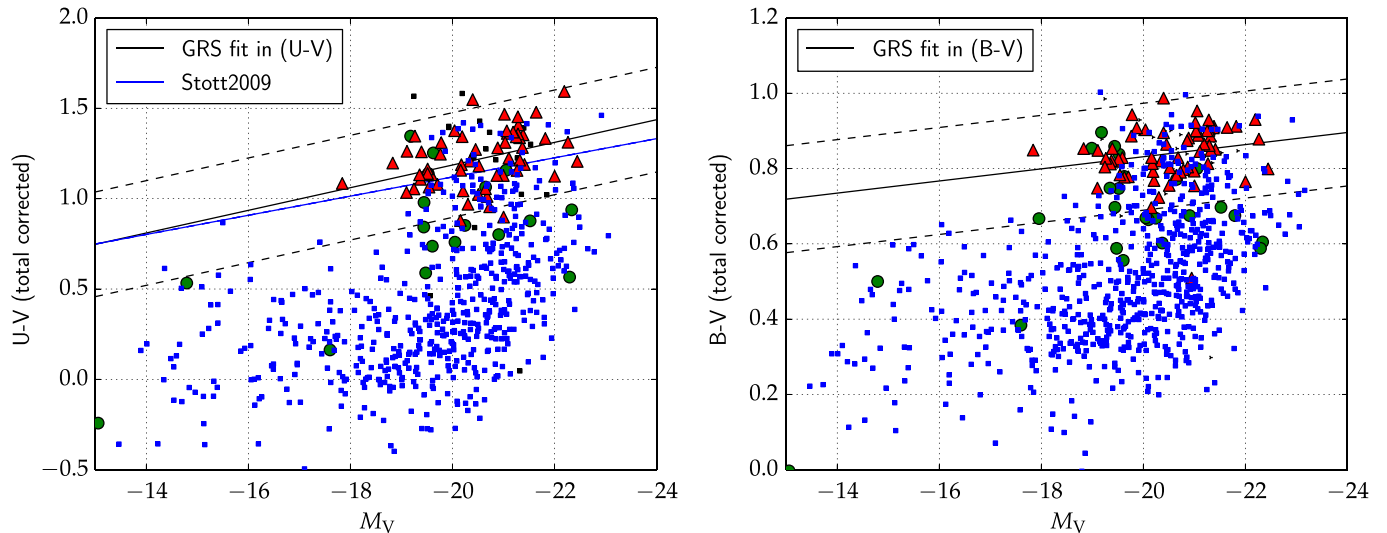


Figure 2. GBS (blue squares), GGV (green points), and GRS (red triangles) galaxies are shown, with a linear fit to the GRS galaxies (solid lines) and the $\text{rms}_{\text{GRS}} = 2$ (dashed lines). Left: optical CMD ($U - V$) vs. V -band absolute magnitude of our sample. The solid blue line is the red-sequence fit from Stott et al. (2009) with the intercept value adjusted for comparison. Right: ($B - V$) vs. V -band absolute magnitude.

position of our GBS, GRS, and GGV galaxies using blue, red, and green points, respectively (Figure 1).

Despite the low number of GGV galaxies overall, they fall either on the optical red sequence (RS) or on the (ill-defined) optical green valley (GV), with only a very few being optically blue galaxies. This result indicates that GGV galaxies are evolving *off* the GBS much slower in ($\text{NUV} - [3.6]$) than in ($\text{FUV} - \text{NUV}$), while the optical colors are reddened by more than $[0.4 \text{ mag}]$ 0.2 mag in $[(U - B)]$ ($B - V$). Alternatively, the GGV galaxies are optically red systems that are growing a disk (*toward* the GBS), in which case the optical reddening is less than $[0.3 \text{ mag}]$ 0.2 mag in $[(U - B)]$ ($B - V$).

It is interesting to note that the majority of the galaxies in the optical GV belong to the GBS, i.e., they are star-forming systems to be classified as such at UV wavelengths. The same can be said about the blue dots found in Figure 2 near the optical RS. This means that either they are in the tail end of star formation or they are regrowing a disk. In particular, a disk regrowth is unlikely, given that the GGV galaxies are found preferentially in dense environments where such a process may be more difficult than in the outskirts of a cluster or a lower-density environment (Section 4.3).

By using the classification of interacting systems within S^4G given by Knapen et al. (2014), we do not find a clear difference between the fraction of close interactions in the three regions of our color-color diagram. When splitting the sample by level of interaction and morphological type, low number statistics hamper determining, for example, whether or not E/S0 in the GGV are mergers or post-starbursts.

4. DISCUSSION

4.1. Modeling Color Evolution

In Figure 3 (left), we show single stellar population (SSP) models (initial mass function, IMF: Chabrier) of S. Charlot & G. Bruzual (2007, private communication) for different metallicities and ages. For all cases, the ($\text{FUV} - \text{NUV}$) color becomes redder until it reaches a peak (at about 1 Gyr in the case of solar metallicity), and then becomes bluer again (UV-

upturn) as the models age. For these SSP models, the color transition from GBS to GRS takes less than a few 10^8 yr .

To better understand what drives the position of galaxies in the color-color diagram, we use a grid of disk galaxy models from Boissier & Prantzos (2000) with various circular velocities V_c and spin parameters λ (Figure 3, right). These models span the entire GBS due to their variation in the star formation timescale with V_c and λ . Besides, the reddening arrow points along the GBS, so internal extinction contributes little to its spread since the star formation timescale and dust attenuation are nearly degenerate in these colors (Section 4.2). The tightness of the GBS is also due to the fact that the effects of an episodic SFH in the $\text{FUV} - \text{NUV}$ color (compared to the $\text{NUV} - [3.6]$) are only expected at very low masses (typically rather blue $\text{NUV} - [3.6]$ colors). Noteworthy examples of this are PGC 065367 or ESO 245-007. To produce more realistic galaxy colors, we add a bulge to the Boissier & Prantzos (2000) disks using SSP predictions with ages between 10^9 and $10^{10.3} \text{ Gyr}$ and a different formation timescale τ . We adopt a bulge model with ($\text{NUV} - [3.6]$) = 5.3 mag and ($\text{FUV} - \text{NUV}$) color = 2.4 mag.

Three of these “disk + bulge” models are shown in Figure 3 (right) for various bulge-to-total mass ratios B/T . Each colored line represents the colors of the resulting galaxy model for B/T from 0.0 to 0.5 in steps of 0.1. Adding a BC03 SSP-based bulge to any of our disk models does not reproduce the reddening in ($\text{FUV} - \text{NUV}$) observed in numerous early-type spirals unless we assume a very high B/T (typical observed B/T of S0 and S0-a galaxies are below 30%; Laurikainen et al. 2007). This shows that the position of transitional early-type spirals is not only due to their (red) massive bulges but also to their disks being red compared to the disks of galaxies in the GBS. This result explains the red ($\text{FUV} - \text{NUV}$) colors of some (transitional) disk galaxies. Whether those disk galaxies could evolve into systems with properties similar to those of current-day ETGs cannot be determined from these data alone.

To analyze the transformation timescale of these disks under a more realistic scenario, we use a model that includes ram-pressure stripping of the gas (hereafter RPS) as a potential mechanism, albeit not the only (potential) one, to redden a

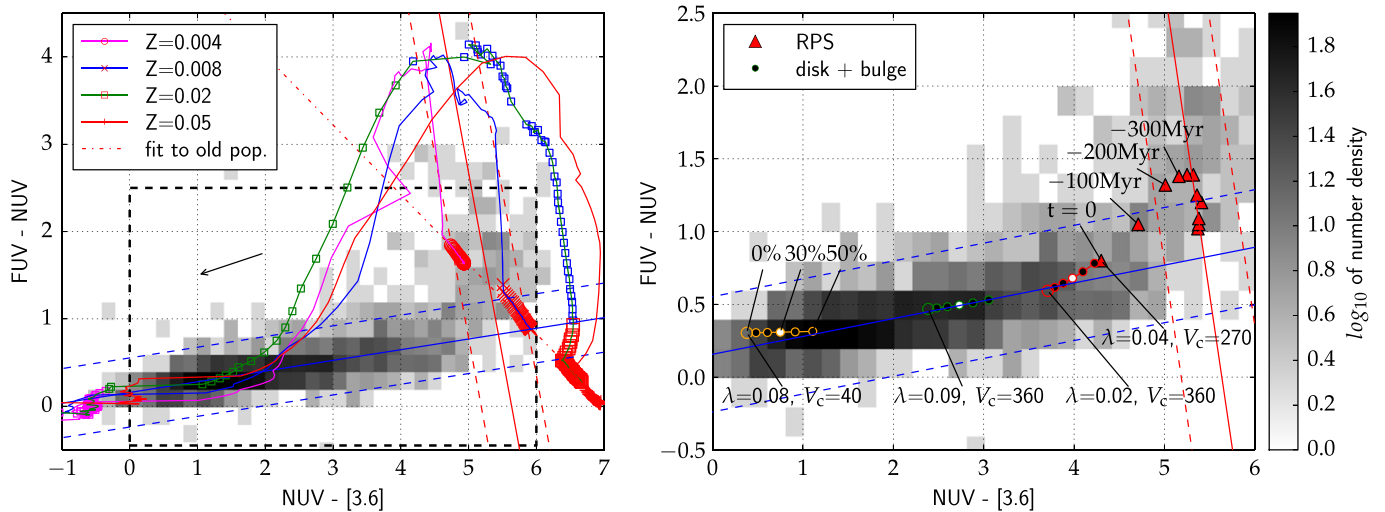


Figure 3. Number density of galaxies in the $(FUV-NUV)$ vs. $(NUV-[3.6])$ color-color diagram, in grayscale-coded 2D bins on a logarithmic scale (see the color bar). Each bin is 0.2×0.2 mag in size. Left : single stellar population (SSP) models (CB07; Chabrier IMF) for various metallicities are overplotted on the number density distribution. The open squares are various age time steps for the model with solar metallicity ($Z = 0.02$), color-coded according to the following $\log(\text{age})$ ranges: magenta, 5.0–8.0; green, 8.0–9.0; blue, 9.0–10.0; and red, 10.0–10.3. The age increases from left to right, from $\log(\text{age}) = 5.0$ to 10.3, for all models. Evolved model points ($\log(\text{age}) \geq 10.0$) are plotted in red for all models. A linear fit to these points (dash-dotted line) is traced for visual comparison with the slope of the GRS. The black rectangle outlines the region of the right panel. Right : the red triangles at $(NUV-[3.6]) > 4$ are model cluster galaxies under the effect of ram-pressure stripping (RPS; see Boselli et al. 2006) where the annotations indicate when the RPS started (with $t = 0$ being the present). The model indicate that the transition timescale of galaxies from the GBS to the GRS is very short, on the order of a few 10^8 yr. We also show three examples, as orange, green, and red dotted lines, of BP00 + BC03 “disk + bulge” models for various B/T ratios, where each node corresponds to a value of the B/T ratio, namely, 0.0 (i.e., BP00 disk only, open circles), 0.1, 0.2, 0.3, 0.4, and 0.5, progressively giving bluer to redder results. The position of the maximum $B/T = 0.3$ estimated by Laurikainen et al. (2007) for a sample of S0-a galaxies is shown with white dots. An offset of 0.3 magnitude was added to the $(FUV-NUV)$ colors for all model galaxies (see the text). Both BP00 disk models and RPS models are based on the Kroupa 93 IMF.

galaxy disk. This RPS model starts from an unperturbed disk with $V_c = 270 \text{ km s}^{-1}$ and $\lambda = 0.04$ but with additional ram-pressure to fit the properties of the Virgo galaxy NGC 4569 (Boselli et al. 2006). The points represent the epochs when the peak of RPS occurred, with $t = 0$ corresponding to the present. Both the disk models and the peak RPS models are shifted redward by 0.3 mag in $(FUV-NUV)$ to match the observed color-color distribution. The need for an offset has been discussed in Muñoz-Mateos et al. (2011) and is believed to be due to uncertainties in the calibration of the stellar atmospheres used in the spectral synthesis. This latter RPS disk model fits the observed distribution well, especially with a moderate bulge. The transition timescale derived from the GBS to the GRS in this case would again be of the order of a few 10^8 yr.

4.2. Internal Dust Reddening

To analyze the effects of internal dust, we show the reddening in both colors in Figure 1 (left) for $A_V = 0.5$ mag, assuming the attenuation law of Calzetti et al. (1994). This law reproduces well the relation between IR excess and UV color (Gil de Paz et al. 2007). Interestingly, the reddening arrow indicates an almost complete degeneracy in these colors between reddening and a change in the star formation timescale (as illustrated by the models of Boissier & Prantzos 2000). We find no change in the distribution of offsets from the GBS as a function of the galaxies’ axial ratio (not shown), so the (small) spread of the GBS is unlikely to be due to inclination effects.

4.3. Environmental Effects

In Figure 4, we show, superposed on the number density color-color diagram, the distribution of galaxies that are in Virgo or high-density regions (Laine et al. 2014). The relative

abundance of transitional galaxies in the Virgo cluster is higher for the majority of morphological types, suggesting that an environmental effect is present. There are some indications that environment plays a role in determining whether galaxies lie in the GBS, GGV, or GRS. For example, 43% (12 of 28) of Sa galaxies classified as either GRS or GGV are in the Virgo cluster, while only 12% (16 of 137) of those classified as GBS are in Virgo. The relative preference of GGV and GRS galaxies for the Virgo environment is found for each morphological class separately (Table 1); although in some cases, the results are not statistically significant. Finally, although the presence of early-type spirals in the GGV might be related to environment, this might not be simply due to RPS; there might be other, more fundamental drivers (that also depend on environment) that determine the position of galaxies in this color-color diagram and in the optical CMDs. One possibility might be the degree of uniformity of the angular momentum of accreted material, which would segregate galaxies by morphological type, mass, and color in different environments (less uniform accretion having likely occurred in denser environments).

5. CONCLUDING REMARKS

We show that star-forming galaxies form a tight blue sequence in FUV -to-near-IR color-color diagrams (GBS). One could even define a star-forming galaxy (SFG) as an object residing in that sequence. This is a clear advantage over the optical or optical-IR color-magnitude and color-color diagrams where star-forming galaxies are mixed with other types of sources, such as post-starbursts or, in general, galaxies in the *GALEX* green valley (GGV). Sb, Sa, and S0 galaxies are found all across the path between the GBS and the GRS, through the GGV. Their position is not only driven by their stellar mass or

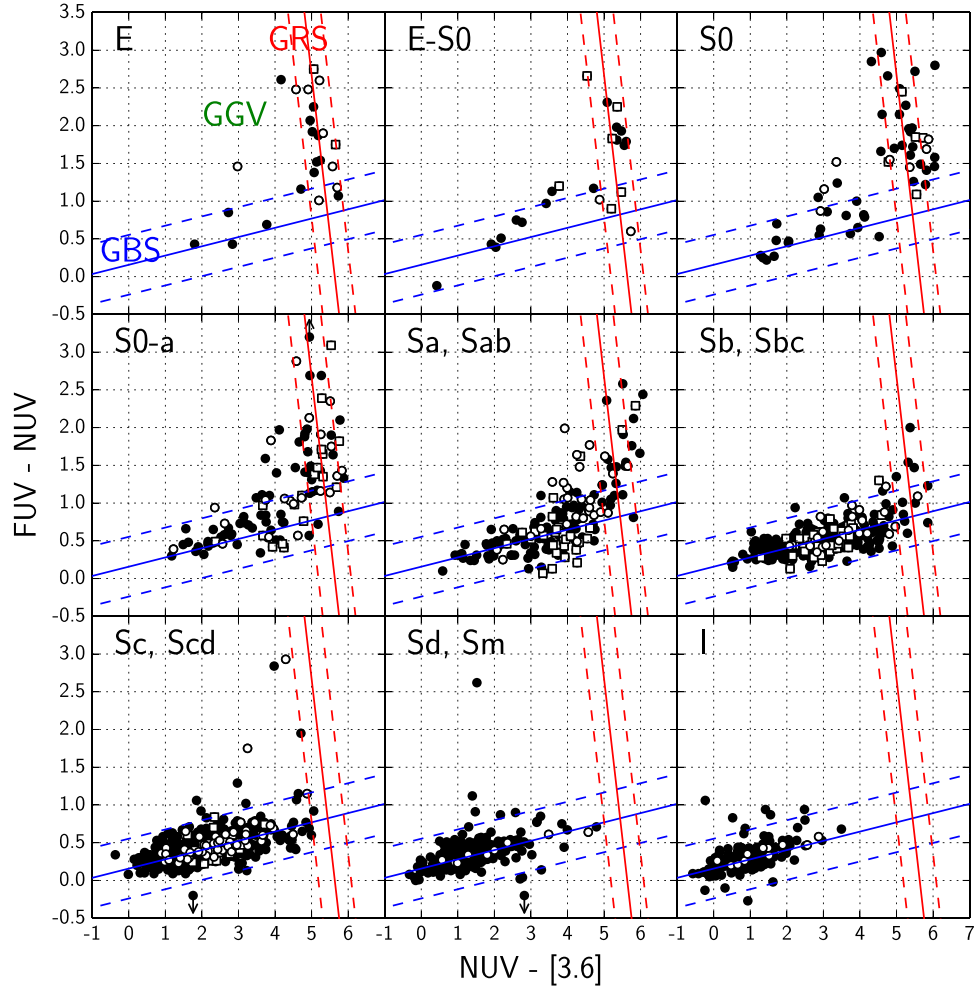


Figure 4. $(FUV-NUV)$ vs. $(NUV-[3.6])$ separated into nine panels by morphological type. Black circles are galaxies with no associated environmental data. Open circles are galaxies in the Virgo cluster. Open squares are galaxies in high-density regions as defined by Laine et al. (2014). The GRS, GGV, and GBS are shown in image E.

Table 1
Counts and Ratios of Virgo Galaxies per Morphological Type Bin per Region

Type ^b	GBS			GGV			GRS			Others ^a			All		
	Virgo ^c	All ^d	Ratio ^e	Virgo	All	Ratio	Virgo	All	Ratio	Virgo	All	Ratio	Virgo	All	Ratio
E	2	7	0.29	2	4	0.50	4	13	0.31	8	24	0.33
E-S0	2	11	0.18	...	4	8	2	23	0.09
S0	1	20	0.05	3	9	0.33	1	15	0.07	2	7	0.33	7	51	0.14
S0-a	11	61	0.18	3	12	0.25	6	24	0.25	2	6	0.22	22	103	0.21
Sa	16	137	0.12	9	14	0.64	3	14	0.21	...	10	...	28	175	0.16
Sb	21	331	0.06	1	5	0.20	...	4	22	340	0.06
Sc	51	656	0.08	2	11	0.18	...	1	1	...	53	669	0.08
Sd	4	162	0.02	...	3	3	...	4	168	0.02
Sm	5	189	0.03	...	2	1	...	5	192	0.03
Irr	11	179	0.06	...	6	1	...	11	186	0.06
ALL types	124	1753	0.07	20	70	0.29	14	79	0.18	4	29	0.14	162	1931	0.08

^a Galaxies where $(FUV-NUV) < 2\sigma$ of the GBS fit and $(NUV-[3.6]) > 1\sigma$ of the GRS fit.

^b Based on Hubble t -type from RC2.

^c From the GOLDMine database (Gavazzi et al. 2003).

^d Including Virgo galaxies.

^e Ratio = Virgo/all.

their bulge mass, but also by the color evolutionary state of their disk. Both SSP and realistic disk + bulge models with RPS indicate that the timescale for the color transition could be as fast as a few 10^8 yr. We cannot determine based solely on the integrated UV, optical, and IR colors of these systems whether they are evolving off or toward the GBS.

The fact that transitioning galaxies are more common in clusters and in high-density regions in general suggests that environment plays a role and is likely to dim their disks. Environment-related mechanisms other than RPS, such as gas starvation (which can start happening in groups; Kawata & Mulchaey 2008), galaxy harassment, or processes related to the degree of uniformity of accretion are all viable. There could be galaxies in the field evolving backwards, i.e., from the GRS toward the GBS, including a large number of optical GV galaxies that we find in the GBS. A future spatially resolved analysis may provide clues to discriminate between these mechanisms since the radial color gradients may be different from one process to another. For example, RPS should lead to strong color gradients as the low-density gas in the outskirts of galaxies would suffer the RPS effects first, while star formation in the inner parts should be unaffected.

The NRAO is a facility of the NSF operated under cooperative agreement by Associated Universities, Inc. We acknowledge financial support to the DAGAL network from the People Programme (Marie Curie Actions) of the European Union's Seventh Framework Programme FP7/2007-2013/ under REA grant agreement number PITN-GA-2011-289313. J.H.K. acknowledges financial support from the Spanish MINECO under grant number AYA2013-41243-P. A.G.d.P.

and J.G. acknowledge financial support under grant number AYA2012-30717.

REFERENCES

- Boissier, S., & Prantzos, N. 2000, *MNRAS*, **312**, 398
 Boselli, A., Boissier, S., Cortese, L., et al. 2006, *ApJ*, **651**, 811
 Boselli, A., Cortese, L., Deharveng, J. M., et al. 2005, *ApJL*, **629**, L29
 Bresolin, F. 2013, *ApJL*, **772**, L23
 Calzetti, D., Kinney, A. L., & Storchi-Bergmann, T. 1994, *ApJ*, **429**, 582
 Cappellari, M., McDermid, R. M., Alatalo, K., et al. 2013, *MNRAS*, **432**, 1862
 Faber, S. M., Willmer, C. N. A., Wolf, C., et al. 2007, *ApJ*, **665**, 265
 Gavazzi, G., Boselli, A., Donati, A., Franzetti, P., & Scodreggio, M. 2003, *A&A*, **400**, 451
 Gil de Paz, A., Boissier, S., Madore, B. F., et al. 2007, *ApJS*, **173**, 185
 Hernández-Pérez, F., & Bruzual, G. 2014, *MNRAS*, **444**, 2571
 Kannappan, S. J., Guie, J. M., & Baker, A. J. 2009, *AJ*, **138**, 579
 Kawata, D., & Mulchaey, J. S. 2008, *ApJL*, **672**, L103
 Knapen, J. H., Erroz-Ferrer, S., Roa, J., et al. 2014, *A&A*, **569**, A91
 Lagos, C. d. P., Davis, T. A., Lacey, C. G., et al. 2014, *MNRAS*, **443**, 1002
 Laine, J., Laurikainen, E., Salo, H., et al. 2014, *MNRAS*, **441**, 1992
 Laurikainen, E., Salo, H., Buta, R., et al. 2007, in IAU Symp. 235, *Galaxy Evolution Across the Hubble Time*, ed. F. Combes, & J. Palouš (Cambridge: Cambridge Univ. Press), **36**
 Martin, D. C., Fanson, J., Schiminovich, D., et al. 2005, *ApJL*, **619**, L1
 Meidt, S. E., Schinnerer, E., van de Ven, G., et al. 2014, *ApJ*, **788**, 144
 Muñoz-Mateos, J. C., Boissier, S., Gil de Paz, A., et al. 2011, *ApJ*, **731**, 10
 Paturel, G., Petit, C., Prugniel, P., et al. 2003, *A&A*, **412**, 45
 Sheth, K., Regan, M., Hinz, J. L., Gil de Paz, A., & Menéndez-Delmestre, K. 2010, *PASP*, **122**, 1397
 Stott, J. P., Pimblett, K. A., Edge, A. C., Smith, G. P., & Wardlow, J. L. 2009, *MNRAS*, **394**, 2098
 Strateva, I., Ivezić, Ž., Knapp, G. R., et al. 2001, *AJ*, **122**, 1861
 Thilker, D. A., Bianchi, L., Schiminovich, D., et al. 2010, *ApJL*, **714**, L171
 Wyder, T. K., Martin, D. C., Schiminovich, D., et al. 2007, *ApJS*, **173**, 293
 Zaritsky, D., Gil de Paz, A., & Bouquin, A. Y. K. 2014, *ApJL*, **780**, L1
 Zaritsky, D., Gil de Paz, A., & Bouquin, A. Y. K. 2015, *MNRAS*, **446**, 2030